Journal of Solid State Chemistry 183 (2010) 2416–2420

Contents lists available at ScienceDirect

Journal of Solid State Chemistry

journal homepage: www.elsevier.com/locate/jssc

Ion-beam irradiation of lanthanum compounds in the systems La_2O_3–Al_2O_3 and La_2O_3–TiO_2

Karl R. Whittle [a,*], Gregory R. Lumpkin [a], Mark G. Blackford [a], Robert D. Aughterson [a], Katherine L. Smith [a], Nestor J. Zaluzec [b]

[a] Institute of Materials Engineering, Australian Nuclear Science and Technology Organisation, PMB 1, Menai, NSW 2234, Australia
[b] Materials Science Division, Argonne National Laboratory, 9700 South Cass Avenue, IL 60439, USA

ARTICLE INFO

Article history:
Received 27 January 2010
Received in revised form
9 July 2010
Accepted 17 July 2010
Available online 2 August 2010

Keywords:
Irradiation
Amorphisation
La_2TiO_5
$La_2Ti_2O_7$

ABSTRACT

Thin crystals of La_2O_3, $LaAlO_3$, $La_{2/3}TiO_3$, La_2TiO_5, and $La_2Ti_2O_7$ have been irradiated *in situ* using 1 MeV Kr^{2+} ions at the Intermediate Voltage Electron Microscope-Tandem User Facility (IVEM-Tandem), Argonne National Laboratory (ANL). We observed that La_2O_3 remained crystalline to a fluence greater than 3.1×10^{16} ions cm^{-2} at a temperature of 50 K. The four binary oxide compounds in the two systems were observed through the crystalline–amorphous transition as a function of ion fluence and temperature. Results from the ion irradiations give critical temperatures for amorphisation (T_c) of 647 K for $LaAlO_3$, 840 K for $La_2Ti_2O_7$, 865 K for $La_{2/3}TiO_3$, and 1027 K for La_2TiO_5. The T_c values observed in this study, together with previous data for Al_2O_3 and TiO_2, are discussed with reference to the melting points for the La_2O_3–Al_2O_3 and La_2O_3–TiO_2 systems and the different local environments within the four crystal structures. Results suggest that there is an observable inverse correlation between T_c and melting temperature (T_m) in the two systems. More complex relationships exist between T_c and crystal structure, with the stoichiometric perovskite $LaAlO_3$ being the most resistant to amorphisation.

1. Introduction

The behaviour of oxide compounds when used for the safe storage of nuclear waste undergoing radioactive decay has been studied as a means to improve current, and develop new waste form materials for future nuclear systems [1]. In order to explain how damage affects a structure it is not always possible to undertake experiments using radioactive isotopes, in many cases it is quicker to use ion-beam irradiation to simulate the short-term aspects of the damage formation and recovery processes [2–4]. While such a technique may not give 'real world' results it does allow 'model' systems to be studied systematically, whose results can then be used to understand currently relevant materials. One area of discussion in the literature is the effect of structure versus composition [3], as part of this process we have studied a number of compounds in the systems La_2O_3–Al_2O_3 and La_2O_3–TiO_2, primarily the binary oxide compounds, $LaAlO_3$, $La_{2/3}TiO_3$, $La_2Ti_2O_7$ and La_2TiO_5. In these systems one must consider both the extent of phase stability field and detail of the different crystal structures as a function of composition, especially within the La_2O_3–TiO_2 system as there are a number of binary oxide phases.

Of the three simple oxide compounds defining the two systems, ion irradiation data have been previously reported for Al_2O_3 in the corundum structure ($R\bar{3}c$) [5,6] and for TiO_2 in the rutile ($P4_2/mnm$), brookite ($Pbca$), and anatase ($I4_1/amd$) modifications [3]. La_2O_3 is one of the five known *A*-type lanthanide oxide compounds ($P\bar{3}m1$) with an atomic configuration that can be described as a rhombohedrally distorted CsCl type structure, e.g., $La_2\square O_3$, in which the La ions occupy a 7-coordinated "monocapped" polyhedron [7].

Within the binary oxide compounds in the two systems, $LaAlO_3$ is a stoichiometric perovskite crystallising in space group $R\bar{3}c$ at room temperature [8]. This compound transforms to the primitive cubic structure at 820 K, which is within the temperature range accessible for ion irradiation experiments in this study. $La_{2/3}TiO_3$, a cation-deficient perovskite, has previously been studied by X-ray and neutron diffraction [9–11] and confirmed to adopt *Cmmm* symmetry, with ordered occupancy of one of the two La^{3+} crystallographic sites, coordinated by either 10 or 12 oxygen anions. In order to maintain charge balance the ten-coordinated La^{3+} site has partial occupancy of 33%, and is randomly ordered. According to the latest phase diagram [10], $La_{2/3}TiO_3$ transforms to the tetragonal ($P4/mmm$) modification above ~640 K, retaining the layered cation-vacancy ordering but not the octahedral tilting as found in the lower temperature form.

$La_2Ti_2O_7$ is isostructural with $Ca_2Nb_2O_7$ with a cation arrangement similar to that of perovskite [12,13]. La^{3+} is located within four different irregular polyhedra with co-ordination numbers ranging from 7 to 11, while the Ti-cations remain octahedrally coordinated by oxygen. Two La^{3+} cations are located within a

* Corresponding author. Fax: +61 2 9543 7179.
E-mail address: karl.whittle@ansto.gov.au (K.R. Whittle).

0022-4596/$ - see front matter © 2010 Elsevier Inc. All rights reserved.
doi:10.1016/j.jssc.2010.07.033

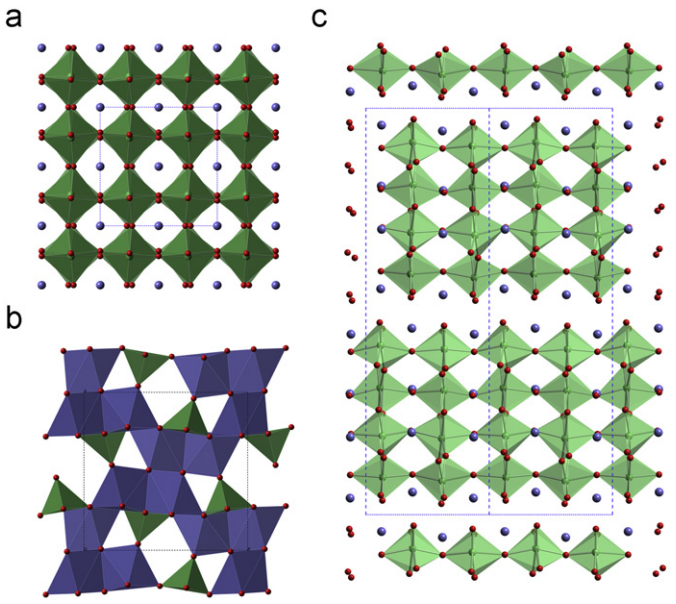

Fig. 1. Crystal representations of (a) $La_{2/3}TiO_3$ viewed down [100], (b) La_2TiO_5 viewed down [001] showing the 5 co-ordinate TiO and 7 co-ordinate LaO, and (c) $La_2Ti_2O_7$ viewed down [001]. The green polyhedra are Ti–O, the purple polyhedra/atoms are La–O.

highly distorted perovskite block while two occupy sites within layers between the perovskite blocks. Adjacent perovskite blocks are offset by a crystallographic shear along the [100] direction, the offset being equivalent to one half of the BO_6 octahedra. This arrangement of atoms results in this material being considered a ferroelectric insulator with $P2_1$ symmetry and a high Curie temperature, ~1770 K.

La_2TiO_5 is orthorhombic and adopts *Pnma* symmetry with atypical La^{3+} and Ti^{4+} co-ordination with oxygen [14–16]. In $La_{2/3}TiO_3$ and $La_2Ti_2O_7$ the La^{3+} co-ordination tends to be large, 7–11, the exact value dependent on the distances used to determine the coordinating anions, while the Ti–O first co-ordination shell is 6 (octahedral). In La_2TiO_5 the La–O co-ordination is 7 and the Ti–O is 5. Such co-ordination gives rise to polyhedral geometries not often seen with these cations, e.g., TiO_5 is an off-centre square-based pyramid. Schematics of each of the structures are shown in Fig. 1.

2. Experimental

The samples used in this study are those that have been previously prepared and characterised [10,17,18]. The compositions of the grains used were checked using TEM-EDX measurements, using method previously published [19], prior to irradiation to minimise any effects due to unexpected compositional changes. *In situ* ion irradiation experiments were performed using a Hitachi H-9000NAR transmission electron microscope (operated at 300 kV) interfaced with a NEC ion accelerator in the IVEM-Tandem User Facility (IVEM) at Argonne National Laboratory (ANL). Firstly, the fluence of 1 MeV Kr^{2+} ions needed to amorphise a reference specimen (Nd-doped zirconolite) at room temperature was measured, to confirm the ion-flux impacting specimens. Progression of damage in samples was measured as a function of ion fluence (F) at different temperatures (T). All samples were irradiated at 50 K; however the other temperatures used were dependent upon radiation response.

Grains selected for monitoring during ion irradiation generally showed many Bragg beams in their selected area diffraction patterns (SADPs). Specimens were alternately irradiated with 1.0 MeV Kr^{2+} ions and then examined in the TEM using the procedure described by Smith et al. [20] to determine the critical fluence for amorphisation (F_c), while removing potential synergistic interactions between the electron and ion beams. Grains were irradiated in random orientations in order to average out any effects of ion channelling. By using SADPs taken at different fluence steps, the average fluence at which all Bragg beams had disappeared and the fluence immediately prior was taken to be F_c. The quoted F_c values in this paper are from 3 or more grains, the quoted errors are representative of the spread in experimental results or the size of the fluence steps, whichever was larger. A Gatan liquid helium (LHe) cooling stage and a Gatan heating stage were used to conduct experiments at temperatures between 30 and 275 K and between room temperature and 1100 K, respectively. The fluence rate was $\leq 6.25 \times 10^{11}$ ion c^{-2} s^{-1}, so that the temperature variation as measured by the temperature controllers was no more than 2 K. The La_2O_3 samples were held at 750 K under vacuum prior to irradiation to remove any unwanted CO_2 or H_2O and rapidly transferred to the cold stage for the ion irradiation experiments, the removal of CO_2/H_2O was confirmed with a diffraction pattern recorded before and after.

3. Results

The results indicate that La_2O_3 retained crystallinity to a fluence above 3.1×10^{16} ions cm^{-2} at 50 K. This result is consistent with the available data reported in the literature for other lanthanide oxides [21], Al_2O_3 [5,6], and the rutile form of TiO_2 [3] with low levels of chemical impurities. As reported earlier [3], anatase, brookite, and chemically impure rutile specimens can be rendered amorphous at 50 K using 1.0 MeV Kr ions. All four of the intermediate binary oxide compounds in the two systems became amorphous when irradiated at 50 K; therefore, additional experiments were conducted at higher temperatures in order to evaluate the kinetics of damage recovery. Representative SADPs recorded at various fluence levels during the irradiations are shown in Fig. 2. With increasing fluence, all four compounds exhibit gradually diminishing Bragg beam intensities in the SADPs, together with a gradual increase in the diffuse scattering from amorphous domains. These diffuse rings appear with equivalent momentum transfers (Q) of ~2.1, 3.5 and 5.3, characteristic of the pair correlation functions for amorphous oxide materials.

The values recorded for F_c at the measured temperatures were fitted using Eq. (1) to obtain the critical temperature for amorphisation (T_c) the temperature at which the recovery rate is equivalent to the damage rate, the intercept fluence at zero K (F_{c0}), and an estimate of the energy of activation (E_a) for recovery from radiation damage [22]

$$F_c = \frac{F_{c0}}{1-\exp[(E_a/k_b)(1/T_c-1/T)]} \quad (1)$$

where T is the temperature of the measurement and k_b is Boltzmann's constant. The intercept fluence F_{c0} is inversely proportional to amorphisation cross-section, e.g., $=1/\sigma_a$ under the conditions of the experiment. Results from this analysis are shown in Table 1, and a plot of the recorded data, errors, and resultant fits are shown in Fig. 3. The data reveal that $La_{2/3}TiO_3$ and $La_2Ti_2O_7$ have similar T_c values of 865 ± 3 and 840 ± 8 K, respectively, while there is a large difference for La_2TiO_5 with a T_c of 1027 ± 10 K. In contrast, the stoichiometric perovskite $LaAlO_3$ returns a significantly different value of 647 ± 3 K.

It has previously been reported that values for E_a given by this equation are often under estimated, when compared with defect migration energies calculated for oxides. This is partly due to the

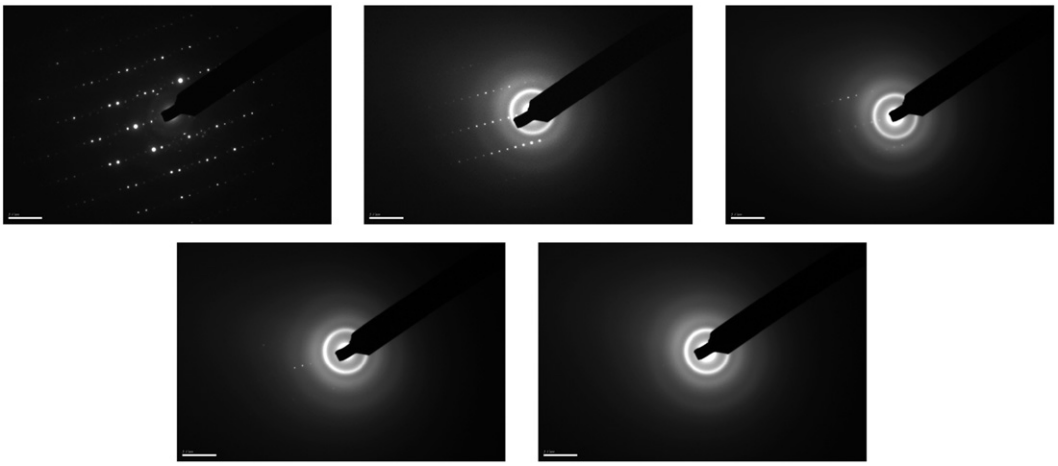

Fig. 2. Recorded selected area diffraction patterns for La_2TiO_5 recorded for fluences of 0, 9.375×10^{13}, 1.563×10^{14}, 2.188×10^{14}, and 5×10^{14} ions cm^{-2} recorded at 300 K.

Table 1
Results from the fitting of recorded data using Eq. (1).

Phase	F_{c0} (10^{14} ions cm^{-2})	Error	T_c (K)	Error	E_a (eV)	Error
$LaAlO_3$	3.66	0.09	646.5	2.5	0.18	0.01
$La_{2/3}TiO_3$	2.57	0.38	864.7	2.8	0.31	0.07
$La_2Ti_2O_7$	2.16	0.11	840.4	7.8	0.44	0.08
La_2TiO_5	1.76	0.08	1027.0	9.5	1.14	0.36

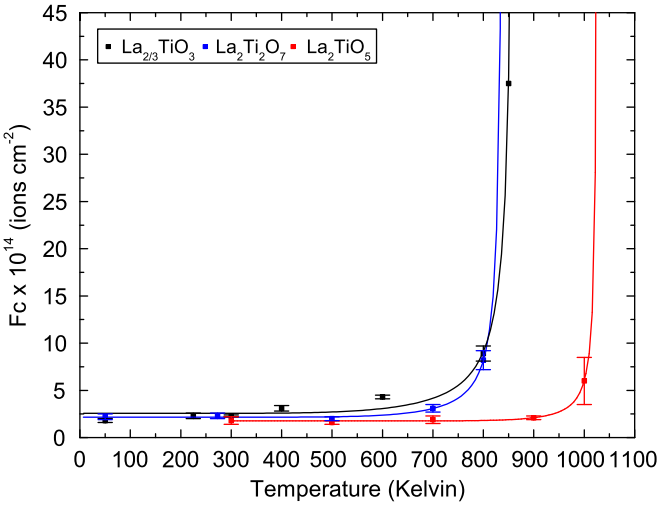

Fig. 3. Plot showing collected data with Eq. (1) fitted, the values obtained from fitting are shown in Table 1. Error bars are present in all points measured.

effect E_a has on the function used to analyse the data. Since this type of irradiation increases damage/amorphous content exponentially with temperature, with F_{c0} being the intercept and T_c being the asymptotic limit, the value obtained for E_a is related to the tipping point of the curve. It takes into account no structural effects on recrystallisation, and as such often gives lower values for E_a than would be expected. As has been suggested previously by Weber [22] these low values are reflective of amorphisation kinetics being controlled by more than one process. In addition one cannot rule out the potential effects of the large surface area in very thin TEM specimens. An alternative method for determining E_a is based on amorphisation cross-sections, ion-flux and jump frequency [22]

$$T_c = \frac{E_a}{k_b \ln[F_{c0}\nu/\phi]} \Rightarrow E_a = T_c\left[k_b \ln\left[\frac{F_{c0}\nu}{\phi}\right]\right] \quad (2)$$

where T_c and F_{c0} are those values determined from Eq. (1), but which can be estimated from direct examination of the data, ν is the effective jump frequency in these samples, an estimated value of 10^{12} was used, and ϕ is the ion-flux (6.25×10^{11} ions cm^{-2} s^{-1}). However, for this process to be valid good estimates of F_{c0}, T_c (obtainable from Eq. (1)) and the known ion-flux (ϕ) are required. The results from this analysis are shown in Table 2.

Table 2
Results from application of Eq. (2) to data obtained from previous analysis, shown in Table 1.

Phase	E_a (eV)	Error
$LaAlO_3$	1.89	0.01
$La_{2/3}TiO_3$	2.51	0.02
$La_2Ti_2O_7$	2.42	0.03
La_2TiO_5	2.94	0.03

4. Discussion

When the values for F_{c0} are compared (Table 2) it can be seen that La_2TiO_5, which has the highest T_c, has the lowest F_{c0}, whereas $LaAlO_3$ with the lowest T_c has the highest F_{c0}. As the critical fluence at 0 K is inversely related to the amorphisation cross-section, $LaAlO_3$, thermodynamically, should recover more rapidly than La_2TiO_5 at 0 K.

When the nuclear and electronic stopping powers for these systems are calculated, for 1 MeV Kr using SRIM2008 [23], the values for the La–Ti–O systems are as expected similar while $LaAlO_3$ is markedly different. For example, the electronic to nuclear stopping ratio (ENSP), the degree of interaction between atomic nuclei or electron clouds on the irradiation ion, for the La–Ti–O systems are ~0.8, while for $LaAlO_3$ the value is 1.27. Values <1 indicate that nuclear interactions decrease the momentum of the incoming ion, >1 indicates electronic effects dominate. Since the calculated stopping factors are close, it would be expected that the T_c for La–Ti–O materials would be similar if only the electronic/nuclear interactions determined a systems

Table 3
Results obtained from SRIM2008 simulation of previously published structures. ENSP refers to the ratio of electronic to nuclear stopping factors.

System	Density (g cm^{-3})	(Atoms cm^{-3})	dE/dx-elec (keV μm^{-1})	dE/dx-nucl (keV μm^{-1})	ENSP	Projected range (Å)
$La_{2/3}TiO_3$	5.35	7.79×10^{22}	9.92×10^{2}	1.24×10^{3}	0.8	3614
$La_2Ti_2O_7$	5.5	7.50×10^{22}	10.24×10^{2}	1.27×10^{3}	0.81	3457
La_2TiO_5	5.78	6.87×10^{22}	9.10×10^{2}	1.13×10^{3}	0.81	3820
$LaAlO_3$	6.522	9.18×10^{22}	18.10×10^{2}	1.42×10^{2}	1.27	3043
La_2O_3	6.56	6.06×10^{22}	9.73×10^{2}	1.19×10^{3}	0.81	3457

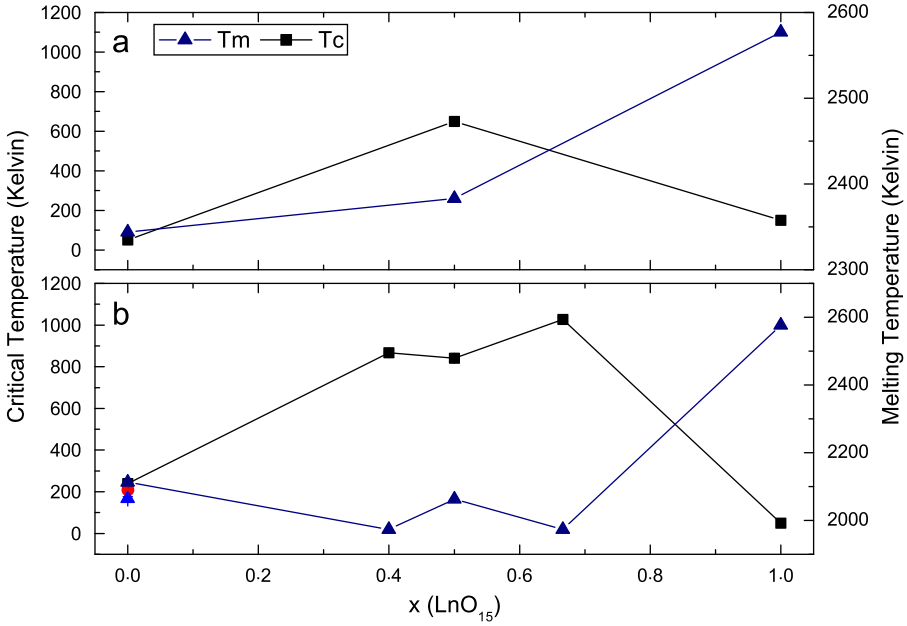

Fig. 4. Comparison between the critical temperature for amorphisation (T_c) and the melting point (T_m) in the systems: (a) La_2O_3–Al_2O_3 and (b) La_2O_3–TiO_2.

response. Since they are not there are other factors affecting stability such as structure.

$La_2Ti_2O_7$, $La_{2/3}TiO_3$, and $LaAlO_3$ all adopt perovskite related structures. As such they can be expected, and shown here, to have similar responses to radiation damage. $LaAlO_3$ has a lower T_c than either $La_{2/3}TiO_3$ or $La_2Ti_2O_7$ most likely due to the change in composition from Ti to Al, and the internal bonding landscape. The outlier in these results is La_2TiO_5 with the atypical co-ordinations for both La and Ti.

As outlined in the introduction $La_{2/3}TiO_3$ (which can be represented as $La_2Ti_3O_9$) and $La_2Ti_2O_7$ adopt similar structures, as such they would be expected to have similar responses to irradiation. Since these structures are perovskite or closely related to perovskite, they have similar unit cell and atomic densities. $LaAlO_3$ has higher densities, both unit cell and atomic, due to the close packed nature of the structure and has a filling factor of ~0.8 (based on ionic radii [24]). The values are shown in Table 3. La_2TiO_5 adopts a different structure with atypical cation–oxygen co-ordinations of 7 (La–O) and 5 (Ti–O), this difference gives rise to a higher mass density, but lower atomic density, Table 3. The lowering in atomic density for La_2TiO_5 correlates with the atypical co-ordination for La and Ti, and directly relates to 'voids' formed from 'incompletely' formed polyhedra. These voids can act as defect sinks during the recovery from damage processes, and provides volumes by which intermediate structures can be adopted. If the determining factor in these systems was the Ti–O co-ordination alone then indeed the T_c's would be similar. However, in the $Ln_2Ti_2O_7$ (Ln=Gd–Lu) series of pyrochlore [25], where Ti–O is 6 co-ordinate, the T_c's decrease as the Ln changes from Gd to Lu.

When the melting points for each of the phases being irradiated are compared with the determined T_c an inverse relationship is found, with the end members, e.g., La_2O_3, having the lowest T_c, but the highest melting point. This is particularly observable for the La_2O_3–TiO_2 system (Fig. 4b). The linkage between amorphisation and melting point has previously been discussed by Naguib and Kelly [26]. If the impacting ion is of sufficient energy or mass, the impact can be considered to locally melt the sample, constrained within the crystalline matrix, similar to that outlined [3] for TiO_2. Upon formation this liquid-like state will cool, e.g. $t^{-3/2}$, the rate of which will be related to the surrounding temperature and diffusion rate. Effectively the higher the temperature above the melting point the longer the sample will remain liquid-like. As the sample cools and drops below the melting point the sample will begin to regain crystallinity, i.e. the higher the melting point the earlier the sample will begin to crystallise. In the samples studied here the binary oxides, La_2O_3, Al_2O_3, and TiO_2 have the highest melting points, and the lowest T_c's for damage. Conversely the ternary oxides, e.g. La_2TiO_5 and $LaAlO_3$ have much lower melting points, and higher T_c's for damage. Similar observation have been made by Lam et al. [27,28], who using Lindemann criteria for melting show that increasing static atomic disorder is thermodynamically equivalent to heating. Thus the melting point of disordered materials would be expected to decrease as disorder increases.

A final explanation for the difference in stability can be related to disorder, both chemical and structural. During thermally assisted recovery the expected structure adopted would be that with the lowest free energy, therefore structures with intrinsic site disorder should have a lower T_c than highly ordered

structures. This is based on the assumption of no element partitioning or preference for an atom type to occupy an identical crystallographic site to that from which it was displaced, i.e. 1 Ti site is as good as any other. For example in $La_2Ti_2O_7$ there are 4 La–O crystallographic sites, which have different local co-ordinations. Therefore, it would be energetically easy for a La cation to be 'knocked' off position and recover to a different La crystallographic site requiring lower temperatures/activation energies for complete recovery, than a highly ordered structure. If this approach is applied to La_2TiO_5, then when a cation is 'knocked' of position and a defect region is formed, there is only 1 ideal crystallographic position that can be adopted for structural recovery. There is of course the possibility of anti-site occupancies however, they are unlikely to occur due to size constraints, i.e. Ti^{4+} is a much smaller cation [24] than La^{3+}, in octahedral co-ordination Ti^{4+} is 0.605 Å, while La^{3+} is 1.032 Å. Once formed such anti-site occupancies would start to destabilise the structure, reducing of the stability. In addition to size effects, the 'void' space acts as a defect sink, similar to those found in the polymorphs [3] of TiO_2, which again begin to destabilise the ideal crystal structure. In such a regime thermally assisted recovery, where recovery is at the same rate as disorder/defect formation, would require a higher temperature. This is particularly apt for those systems with high degrees of site preference, particularly when effects such as orbital overlap [29,30], which are both energetically and geometrically constrained, are included.

5. Conclusion

The results indicate that changes in crystal structures directly affect the response to radiation damage of materials, e.g. La_2TiO_5 and $La_2Ti_2O_7$, while being chemically similar have different responses to radiation damage. The variations can be related to crystal structure, chemical and structural disorder and in these systems an inverse correlation with melting point is found. This work is being expanded to include MD simulations of damage and recovery processes for other ternary oxides, e.g. Y–Ti–Sn–O.

References

[1] W.J. Weber, R.C. Ewing, C.R.A. Catlow, T.D. de la Rubia, L.W. Hobbs, C. Kinoshita, H. Matzke, A.T. Motta, M. Nastasi, E.K.H. Salje, E.R. Vance, S.J. Zinkle, Journal of Materials Research 13 (6) (1998) 1434–1484.
[2] R.C. Ewing, W.J. Weber, J. Lian, Journal of Applied Physics 95 (2004) 5949–5972.
[3] G.R. Lumpkin, K.L. Smith, M.G. Blackford, B.S. Thomas, K.R. Whittle, N.A. Marks, N.J. Zaluzec, Physical Review B 77 (21) (2008) 212401.
[4] G.R. Lumpkin, J.M. Pruneda, S. Rios, K.L. Smith, K. Trachenko, K.R. Whittle, N.J. Zaluzec, Journal of Solid State Chemistry 180 (4) (2007) 1512–1518.
[5] G.P. Pells, Journal of the American Ceramic Society 77 (2) (1994) 368–371.
[6] R. Devanathan, J.N. Mitchell, K.E. Sickafus, W.J. Weber, M. Nastasi, Materials Science and Engineering A 253 (1) (1998) 131–134.
[7] L. Marsella, V. Fiorentini, Physical Review B 69 (17) (2004) 4.
[8] C.J. Howard, B.J. Kennedy, B.C. Chakoumakos, Journal of Physics—Condensed Matter 12 (4) (2000) 349–365.
[9] K.L. Smith, G.R. Lumpkin, M.G. Blackford, M. Colella, N.J. Zaluzec, Journal of Applied Physics 103 (2008) 083531.
[10] Z. Zhang, G.R. Lumpkin, C.J. Howard, K.S. Knight, K.R. Whittle, K. Osaka, Journal of Solid State Chemistry 180 (3) (2007) 1083–1092.
[11] C.J. Howard, G.R. Lumpkin, R.I. Smith, Z. Zhang, Journal of Solid State Chemistry 177 (2004) 2733–2739.
[12] H.W. Schmalle, T. Williams, A. Reller, A. Linden, J.G. Bednorz, Acta Crystallographica, Section B—Structural Science 49 (1993) 235–244.
[13] N. Ishizawa, F. Marumo, S. Iwai, M. Kimura, T. Kawamura, Acta Crystallographica, Section B—Structural Science 38 (1982) 368–372.
[14] M.A. Petrova, A.S. Novikova, R.G. Grebenshchikov, Inorganic Materials 39 (5) (2003) 509–513.
[15] S.D. Skapin, D. Kolar, D. Suvorov, Journal of the European Ceramic Society 20 (8) (2000) 1179.
[16] H. Muller-Buschbaum, K. Scheunemann, Journal of Inorganic and Nuclear Chemistry 35 (4) (1973) 1091–1098.
[17] R.D. Aughterson, G.R. Lumpkin, K.L. Smith, G.J. Thorogood, K.R. Whittle, in: W.E. Lee, J.W. Roberts, N.C. Hyatt, R.W. Grimes (Eds.), Scientific Basis for Nuclear Waste Management, vol. XXXI, Materials Research Society, Sheffield, 2007, pp 365–370.
[18] E.J. Harvey, K.R. Whittle, G.R. Lumpkin, R.I. Smith, S.A.T. Redfern, Journal of Solid State Chemistry 178 (3) (2005) 800–810.
[19] K.R. Whittle, L.M. Cranswick, S.A.T. Redfern, I.P. Swainson, G.R. Lumpkin, Journal of Solid State Chemistry 182 (3) (2009) 442–450.
[20] K.L. Smith, N.J. Zaluzec, G.R. Lumpkin, Journal of Nuclear Materials 250 (1997) 36–52.
[21] M. Tang, J.A. Valdez, P. Lu, G.E. Gosnell, C.J. Wetteland, K.E. Sickafus, Journal of Nuclear Materials 328 (1) (2004) 71–76.
[22] W.J. Weber, Nuclear Instruments & Methods in Physics Research, Section B—Beam Interactions with Materials and Atoms 166–167 (2000) 98–106.
[23] J.F. Ziegler, Nuclear Instruments & Methods in Physics Research, Section B—Beam Interactions with Materials and Atoms 219–220 (2004) 1027–1036.
[24] R.D. Shannon, Acta Crystallographica, Section A A32 (1976) 751–767.
[25] J. Lian, J. Chen, L. Wang, R. Ewing, J. Farmer, L. Boatner, K. Helean, Physical Review B 68 (13) (2003) 134107.
[26] H.M. Naguib, R. Kelly, Radiation Effects 25 (1975) 1–12.
[27] N. Lam, P. Okamoto, M. Li, Journal of Nuclear Materials 251 (1997) 89–97.
[28] N.Q. Lam, P.R. Okamoto, Surface and Coatings Technology 65 (1994) 7–14.
[29] K. Sickafus, L. Minervini, R. Grimes, J. Valdez, M. Ishimaru, F. Li, K. McClellan, T. Hartmann, Science 289 (5480) (2000) 748.
[30] K.R. Whittle, G.R. Lumpkin, K.L. Smith, M.G. Blackford, N.J. Zaluzec, E.J. Harvey, in: D.S. Dunn, C. Poinssot, B. Begg (Eds.), Scientific Basis For Nuclear Waste Management, vol. XXX, Boston, US, 2007, 2006, Materials Research Society, Boston, US, 2006, pp. 0985-NN09-02.